



# A three-equation model for the prediction of soot emissions in LES of gas turbines

Benedetta Franzelli, A. Vié, N. Darabiha

## ► To cite this version:

Benedetta Franzelli, A. Vié, N. Darabiha. A three-equation model for the prediction of soot emissions in LES of gas turbines. Proceedings of the Combustion Institute, 2018, 10.1016/j.proci.2018.05.061 . hal-01856557

HAL Id: hal-01856557

<https://hal.science/hal-01856557>

Submitted on 12 Aug 2018

**HAL** is a multi-disciplinary open access archive for the deposit and dissemination of scientific research documents, whether they are published or not. The documents may come from teaching and research institutions in France or abroad, or from public or private research centers.

L'archive ouverte pluridisciplinaire **HAL**, est destinée au dépôt et à la diffusion de documents scientifiques de niveau recherche, publiés ou non, émanant des établissements d'enseignement et de recherche français ou étrangers, des laboratoires publics ou privés.

# A three-equation model for the prediction of soot emissions in LES of gas turbines

B. Franzelli<sup>a,\*</sup>, A. Vié<sup>a</sup>, N. Darabiha<sup>a</sup>

<sup>a</sup>*Laboratoire EM2C, CNRS, CentraleSupélec, Université Paris-Saclay, 3 rue Joliot Curie, 91192 Gif-sur-Yvette Cedex, FRANCE*

---

## Abstract

*The design of new low-emission systems requires the development of models providing an accurate prediction of soot production for a small computational cost. In this work, a three-equation model is developed based on mono-disperse closure of the source terms from a sectional method. In addition, a post-processing technique to estimate the particles size distribution (PSD) from global quantities is proposed by combining Pareto and log-normal distributions. After validation, the developed strategy is used to perform a large eddy simulation of soot production in a model combustor representative of gas turbine combustion chambers. It is shown that the three-equation model is able to provide a good estimation of soot volume fraction and information on PSD in complex geometries for a low computational time.*

*Keywords:*

Soot modelling, three-equation model, Particle Size Distribution, gas turbine

---

\*Corresponding author:

Email address: [benedetta.franzelli@cnrs.fr](mailto:benedetta.franzelli@cnrs.fr) (B. Franzelli)

## 1. Introduction

Numerical simulations of soot production are essential to design low-emission burners, but require the development of reliable models. This is a challenging task because of the complexity of soot physics, which leads to a poly-disperse population of particles with complex morphologies. Moreover, models should require a minimal CPU cost to perform parametric studies of realistic configurations using Large Eddy Simulation (LES).

Different methods have been applied to LES of sooting turbulent flames with increasing accuracy and CPU cost. Semi-empirical models [1] transport two quantities, generally soot mass fraction and total number density, whose source terms are chosen 'ad hoc' and fitted to experimental data, so that their validity is limited. They rely on a spherical assumption for soot particles and they do not give access to the number density function (NDF). However, their low CPU cost and ease of implementation into CFD solvers have made them preferred candidates for the investigation of complex configurations [2, 3]. Alternatively, methods of moments (MOM) solve the  $N$  first moments of the NDF, the main issue being to compute their source terms, which requires untransported moments. In the Hybrid MOM (HMOM) [4], this is done using an algebraic relationship between moments [5]. This method has been used to simulate turbulent complex configurations [6–8]. However, even if HMOM accounts for soot fractality, the NDF is not accessible. Finally, the sectional method (SM) discretizes the NDF into a discrete number of sections. The soot mass fraction of each section is transported. This method gives access to the NDF and has already been used for LES of model combustors [9]. However, it is highly CPU-time demanding since at least 25 sections are required for a reasonable accuracy. In addition, extension to fractality requires even more

transport equations.

Here, the objective is to develop a three-equation (3-eq) model that accounts for soot fractality and gives an accurate prediction of soot global quantities and an estimation of the NDF for a small CPU cost. The governing equations are presented in Sec. 2, accounting for soot fractality. A strategy to estimate the NDF based on an analysis of NDF shapes obtained with SM simulations is proposed in Sec. 3. In Sec. 4, the 3-eq model is validated in terms of global quantities and NDF reconstruction. Finally, in Sec. 5, the 3-eq model is used in a LES of the model combustor FIRST [10]. This configuration is considered today as a reference for the investigation of soot production under conditions representative of gas turbines. Results are validated against experiments and the convenience of the NDF reconstruction method is discussed.

## 2. The three-equation model

The soot particle population is described by the NDF,  $f(t, x, v, s)$ , giving the particles number density at volume  $v$  and surface  $s$ .

Total number density  $N_s = \langle f \rangle$ , soot volume fraction  $f_v = \langle vf \rangle$  and total soot surface  $S_s = \langle sf \rangle$  are moments of the NDF, where  $\langle \Phi \rangle = \int \int \Phi dv ds$ . The mean particle volume and surface are  $v_s = f_v N_s^{-1}$  and  $s_s = S_s N_s^{-1}$ , respectively.

Here, a model is developed to describe the global characteristics of soot population, such as  $f_v$  and  $N_s$ , for a small CPU cost. This model is based on the transport of three global variables:  $N_s$ ,  $S_s$  and the soot mass fraction  $Y_s = \rho_s \rho^{-1} f_v$  ( $\rho$  and  $\rho_s$  are the gas and soot density, respectively). Each of these three quantities is

solved using the following equation:

$$\frac{\partial \Psi}{\partial t} + \nabla \cdot (\mathbf{u}\Psi) = \nabla \cdot \left( C_{th} \nu \frac{\nabla T}{T} \Psi \right) + \dot{\omega}_\Psi \quad (1)$$

where  $\mathbf{u}$ ,  $\nu$  and  $T$  are the gas velocity, kinematic viscosity and temperature,  $\rho_s = 1800 \text{ kg m}^{-3}$ , and  $C_{th} = 0.55$  in the limit of small particles with respect to the mean free path of the gas phase [11]. The source terms  $\dot{\omega}_\Psi$  are derived from the sectional model in [12] by assuming a mono-disperse distribution  $f(v, s) = N_s \delta_{v_s} \delta_{s_s}$  ( $\delta$  is the Dirac's delta function):

$$\begin{aligned} \frac{\dot{\omega}_{Y_s}}{\rho_s} &= \underbrace{v_{\text{dim}} \beta_{v_{\text{dim}}}^{\text{fm}} N_{\text{dim}}^2}_{\text{nucleation}} + \underbrace{v_{\text{dim}} \beta_{v_{\text{dim}}, v_s}^{\text{fm}} N_{\text{dim}} N_s}_{\text{condensation}} \\ &\quad + \underbrace{v_{C_2} \lambda k_{\text{sg}} s_s N_s}_{\text{surface growth}} - \underbrace{v_{C_2} \lambda k_{\text{ox}} s_s N_s}_{\text{surface oxidation}} \\ \dot{\omega}_{N_s} &= \underbrace{\frac{\beta_{v_{\text{dim}}}^{\text{fm}} N_{\text{dim}}^2}{2}}_{\text{nucleation}} - \underbrace{(1 - \mathcal{H}[v_s - v_{C_2}]) \lambda k_{\text{ox}} s_s N_s}_{\text{surface oxidation}} - \underbrace{\frac{\beta_{v_s} N_s^2}{2}}_{\text{coagulation}} \\ \dot{\omega}_{S_s} &= \underbrace{(18\pi)^{1/3} (v_{\text{dim}})^{2/3} \beta_{v_{\text{dim}}}^{\text{fm}} N_{\text{dim}}^2}_{\text{nucleation}} + \underbrace{\delta s_{v_{\text{dim}}}^{\text{frac}} \beta_{v_{\text{dim}}, v_s}^{\text{fm}} N_{\text{dim}} N_s}_{\text{condensation}} \\ &\quad + \underbrace{\delta s_{v_{C_2}}^{\text{frac}} \lambda k_{\text{sg}} s_s N_s}_{\text{surface growth}} - \underbrace{\delta s_{v_{C_2}}^{\text{spher}} \lambda k_{\text{ox}} s_s N_s}_{\text{surface oxidation}}, \end{aligned} \quad (2)$$

where  $\mathcal{H}[v]$  is the Heaviside function and  $v_{C_2}$  is the volume of two carbon atoms. Spherical dimers are assumed for nucleation, whose number density  $N_{\text{dim}}$  is computed using a quasi-steady state approximation from the collision of polycyclic aromatic hydrocarbons (PAHs) [13]. For condensation and surface growth, a particle volume variation  $\delta v$  leads to a particle surface variation  $\delta s_{\delta v}^{\text{frac}}$  following a

fractal behavior  $\frac{\delta s_{\delta v}^{\text{frac}}}{s_s} = \frac{2}{3} \frac{\delta v}{v_s} n_p^\chi$  [4], where  $n_p = (36\pi)^{-1} v_s^{-2} s_s^3$  is the number of primary particles and  $\chi = -0.2043$ . As in [4], oxidation modifies the surface of a factor  $\delta s_{\delta v}^{\text{spher}}$  defined as  $\frac{\delta s_{\delta v}^{\text{spher}}}{s_s} = \frac{2}{3} \frac{\delta v}{v_s}$ . The surface reactions constants  $k_{\text{sg}}$  and  $k_{\text{ox}}$  are obtained from the HACA-RC mechanism as in [12].  $\lambda = 1/s_{C_2}$  is the number of active sites per unit surface, where  $s_{C_2}$  is the surface of two carbon atoms. The collisional rates are modelled as:

$$\begin{aligned}\beta_{v_{\text{dim}}}^{\text{fm}} &= \epsilon_{\text{nu}} \sqrt{\frac{\pi k_b T}{2 \rho_s}} \left( \frac{1}{v_{\text{dim}}} + \frac{1}{v_{\text{dim}}} \right)^{1/2} (d_p^{\text{dim}} + d_p^{\text{dim}})^2 \\ \beta_{v_{\text{dim}}, v_s}^{\text{fm}} &= \epsilon_{\text{cd}} \sqrt{\frac{\pi k_b T}{2 \rho_s}} \left( \frac{1}{v_{\text{dim}}} + \frac{1}{v_s} \right)^{1/2} (d_p^{\text{dim}} + d_c)^2 \\ \beta_{v_s} &= \max \left[ \epsilon_{\text{cg}} \sqrt{\frac{\pi k_b T}{2 \rho_s}} \left( \frac{2}{v_s} \right)^{1/2} (2d_c)^2, \frac{8k_b T}{3\rho\nu} \text{Cu} \right]\end{aligned}\quad (3)$$

with  $\epsilon_{\text{nu}} = 2.5$ ,  $\epsilon_{\text{cd}} = 1.3$ ,  $\epsilon_{\text{cg}} = 2.2$ .  $d_c = d_p n_p^{1/D_f}$  is the collisional diameter,  $d_p = 6v_s s_s^{-1}$  is the primary particle diameter,  $D_f = 1.8$  is the fractal dimension,  $\text{Cu} = 1 + 2.154 \lambda_g d_c^{-1}$  is the Cunningham corrective coefficient and  $\lambda_g$  is the mean free path of the gas phase [12].  $k_b$  is the Boltzmann constant. Subscript or superscript dim stand for dimer properties.

$N_s$ ,  $Y_s$  and  $S_s$  correspond to the 0<sup>th</sup>- and 1<sup>st</sup>-order moments used in the bivariate HMOM [4]. However, the source terms in Eqs. (2) are derived using a mono-disperse NDF where HMOM uses assumptions on the moments themselves. This simplifies its formulation, physical understanding and implementation into CFD solvers. Compared to semi-empirical models, our method is a mono-disperse transcription based on a sectional model. Therefore, the source terms do not follow an 'ad-hoc' law fitted to experiments but they account for the physics included into

the detailed SM.

### 3. Reconstruction of the number density function

The 3-eq model is expected to reproduce the global behavior of the soot population, but no information is available on the particles size distribution (PSD). In order to characterize the PSD, a simple strategy is proposed to estimate the marginal NDF,  $n(v) = \int f(v, s)ds$ , from the transported quantities. For simplicity, in the following we will refer to the marginal-NDF as NDF.

On the one side, fine particles such as metal-oxides are known to be characterized by a self-similar distribution [14, 15], approximately log-normal (LN), significantly simplifying the prediction of the NDF. The same approach has been used to investigate the soot particles distribution in fires [16]. On the other side, as observed in laminar [12, 17] and, only recently, in turbulent flames with experiments [18, 19] and numerical simulations [13], the PSD considerably varies along the flame, starting in a one-peak shape and evolving into a two-peaks distribution along the flame. To verify the validity of the self-similarities assumption for sooting flames, results obtained with a SM [12] are presented in Fig. 1(a). They correspond to the burner-stabilized stagnation laminar premixed C<sub>2</sub>H<sub>4</sub>/Ar/O<sub>2</sub> flame experimentally investigated in [17] for a distance between the burner and the stagnation surface equal to  $H = 10$  mm. These numerical results were already proven to be in good agreement with the experimental data [12]. The discussed transition from one- to two-peaks shape is recognized.

In Fig. 1(b), following [16], the dimensionless NDF,  $\psi(\eta) = nf_v/N_s^2$ , is evaluated at different heights above the burner, where  $\eta = v/v_s$  is the dimensionless volume. Figure 1 shows that a single shape cannot reproduce the NDF along

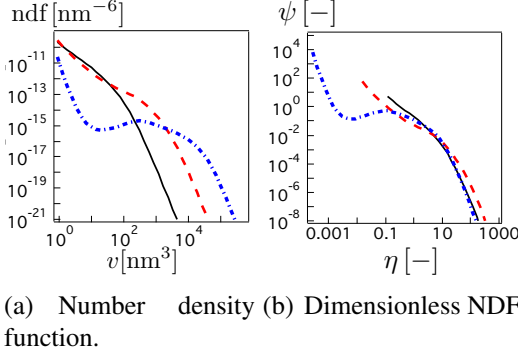


Figure 1: NDF obtained with the SM [12] in a burner-stabilized stagnation laminar premixed C2H4/Ar/O2 flame at three axial positions:  $x = 3 \text{ mm}$  (black line),  $x = 6 \text{ mm}$  (red dashed line) and  $x = 9 \text{ mm}$  (blue dot-dashed line).

the flame. However, we suggest that the PSD can be approximated as the sum of two distributions  $n_1(v)$  and  $n_2(v)$  considering the following normalized NDF,  $\bar{n}(v) = n(v)/N_s$ :

$$\bar{n}(v) \approx \bar{n}_a(v) = \alpha \bar{n}_1(v) + (1 - \alpha) \bar{n}_2(v), \quad (4)$$

where  $\bar{n}_a(v)$  is an approximation of  $\bar{n}(v)$ . By integrating Eq. (4) over the volume, we get:

$$v_s = \alpha v_1^{\text{mean}} + (1 - \alpha) v_2^{\text{mean}}, \quad (5)$$

where  $v_1^{\text{mean}}$  and  $v_2^{\text{mean}}$  are the mean volumes over  $\bar{n}_1$  and  $\bar{n}_2$ , respectively. This implies  $\alpha v_1^{\text{mean}} \leq v_s$  and  $(1 - \alpha) v_2^{\text{mean}} \leq v_s$ . To reproduce the first peak which is mainly due to the growth of the nuclei particles of volume  $v_{\text{nuc}}$ , we consider a Pareto distribution for  $\bar{n}_1(v)$ :

$$\bar{n}_1(v) = k \frac{v_{\text{nuc}}^k}{v^{k+1}} \quad \text{with} \quad v \geq v_{\text{nuc}}, \quad (6)$$

where  $k$  is the Pareto index. In this case,  $v_1^{\text{mean}}$  is analytically given as  $v_1^{\text{mean}} =$

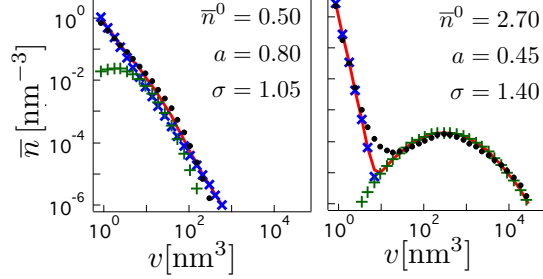


Figure 2: Reconstruction (red continuous line) of the NDF as the sum of a Pareto (blue cross) and a log-normal (green plus) distribution. Results correspond to two axial positions of Fig. 1:  $x = 3$  mm (left),  $x = 9$  mm (right). The reference NDF obtained from a SM is presented as black circles.

$\frac{k}{k-1} v_{\text{nucl}}$ . Assuming that the contribution of  $\bar{n}_2$  is negligible at  $v_{\text{nucl}}$ , Eq. (6) gives the first-peak value as  $\bar{n}^0 = \alpha \bar{n}_1(v_{\text{nucl}}) = \alpha k v_{\text{nucl}}^{-1}$ . Then, given  $\alpha$  and  $\bar{n}^0$ , the Pareto index  $k$  can be obtained as  $k = \max \left[ \bar{n}^0 \alpha^{-1} v_{\text{nucl}}, \epsilon (1 - \alpha v_{\text{nucl}} / v_s)^{-1} \right]$ . This latter criterion guarantees  $\alpha v_1^{\text{mean}} \leq v_s$  (here  $\epsilon = 1.01$ ).

To reproduce the second peak, which is usually observed downstream the flame, due to condensation, coagulation and surface reactions on the biggest particles, an LN function is used for  $\bar{n}_2$  with parameters  $\mu$  and  $\sigma$ :

$$\bar{n}_2(v) = \frac{1}{v\sigma\sqrt{2\pi}} \exp \left( -\frac{(\ln(v) - \mu)^2}{2\sigma^2} \right). \quad (7)$$

Once  $\alpha$  and  $\sigma$  are provided, we get  $\mu = \ln(v_2^{\text{mean}}) - 0.5\sigma^2$ , where  $v_2^{\text{mean}} = (1 - \alpha)^{-1}(v_s - \alpha v_1^{\text{mean}})$ . An example of NDF reconstruction is shown in Fig. 2 for the results corresponding to two axial positions of Fig. 1. As it is observed in Fig. 2, to correctly reproduce the NDF,  $\alpha$ ,  $\bar{n}^0$  and  $\sigma$  have to vary along the flame height. Although NDF evolves as a function of  $f_v$ ,  $N_s$  and  $v_s$ , here we choose  $v_s$  as the best

parameter to trace its shape along the flame and to derive empirical expressions:

$$\alpha = \max \left[ 0, 1.0 - 0.18 \left( \frac{v_s}{v_{\text{nucl}}} \right)^{0.12} \right], \quad (8)$$

$$\bar{n}^0 = 8(1 - \alpha)^2, \quad \sigma = 1 + 0.65(1 - \alpha).$$

Even if constants have been fitted, their evolution is physically justified.  $\alpha$  represents the balance between the Pareto ( $\alpha = 1$ ) and the LN distributions ( $\alpha = 0$ ). As observed experimentally and numerically [12, 14, 15], for small  $v_s$  (and small  $f_v$ ), a one-peak shape is predominant whereas two peaks are retrieved for large mean volumes (and big  $f_v$  values). The evolution of  $\alpha$  captures this trend: the NDF is Pareto-like at the beginning of the flame, evolving towards an LN distribution downstream. The first-peak  $\bar{n}^0$  governs the stiffness of the Pareto distribution. As observed in Fig. 2, the role of the Pareto function is initially to reproduce almost the whole soot population, which is the result of many simultaneous processes, whereas downstream it mainly reproduces only the nuclei production. As a consequence,  $\bar{n}^0$ , meaning  $\bar{n}_1$  stiffness, increases with  $v_s$ . Similarly, the parameter  $\sigma$  is proportional to  $v_s$ . When increasing the volume, the population gathers into the  $\bar{n}_2(v)$  distribution, mainly governed by the coagulation process, leading to a larger value of  $\sigma$ . The proposed reconstruction strategy has been developed by analyzing NDF results from a laminar premixed flame but will be validated in the following on different flame archetypes (laminar and turbulent, premixed and non-premixed flames). Even if the empirical relationships of Eq. (8) may depend on the targeted fuel and/or operating conditions. However, the decomposition into Pareto and LN distributions seems a promising candidate to represent the general transition from one- to two-peaks shapes observed in sooting flames.

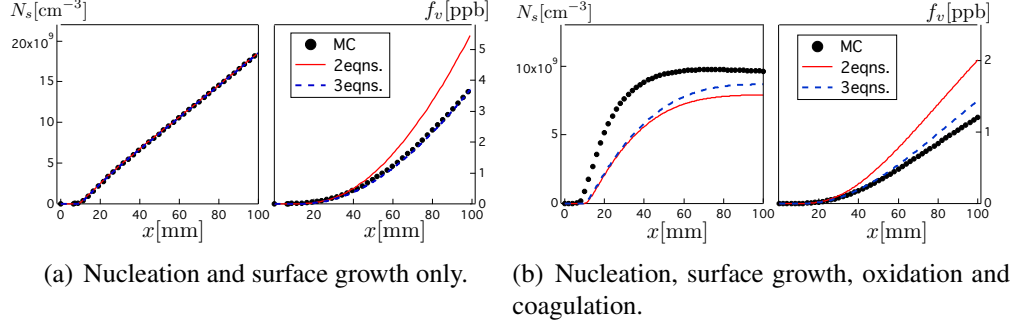


Figure 3: Soot number density (left) and volume fraction (right) in a laminar freely-propagating flame. Results with the 2- and 3-eq models are compared to MC solution (continuous red line, dashed blue line and symbols, respectively).

#### 4. Validation cases

In this session, the 3-eq model is validated against detailed Monte-Carlo or SM simulations. Comparisons with experiments are here avoided since any discrepancy (or agreement) of the 3-eqn model with experiments may potentially depend on the choice of more or less accurate physical and collisional description (in particular to the model's constants), whose evaluation is out of the scope of this work. However, the validation of the 3-eqn model on experimental laminar premixed flames[17] is presented in the supplementary material for completeness.

##### 4.1. Global quantities

The accuracy of the 3-eq model is assessed in a laminar freely-propagating premixed C<sub>2</sub>H<sub>4</sub>/Ar/O<sub>2</sub> flame, simulated with the REGATH solver [20] using the KM2 detailed gas phase reaction mechanism [21] for equivalence ratio  $\phi = 2.1$ , initial temperature  $T = 300$  K and atmospheric pressure. Soot production has been calculated with the 3-eq model as well as a reference Monte-Carlo (MC) approach using the Sweep2 solver [22]. In addition, a two-equation model (2-eq) is also considered by solving Eqs. (1) for  $N_s$  and  $Y_s$  and imposing  $s_s^{2\text{eq}} =$

$(36\pi)^{1/3} v_s^{2/3}$ . In order to guarantee consistency among MC, 3-eq and 2-eq models, spherical particles are considered with MC and  $\delta s^{\text{frac}} = \delta s^{\text{spher}}$  for 3-eq model. First,  $f_v$  and  $N_s$  profiles are presented in Fig. 3(a) by taking into account only nucleation and surface growth.

The 2-eq model overestimates  $f_v$ , whereas the 3-eq model is able to correctly reproduce the soot production, showing that the equation for  $S_s$  is essential to reproduce the evolution of the particle surface and, consequently, of the growth and destruction source terms, even for spherical particles. Then, results obtained while considering also oxidation and coagulation are presented in Fig. 3(b). Discrepancies with the MC profiles are observed since the mono-disperse closure assumption is less valid since the resultant MC soot population is more poly-disperse in this case (not shown). However, the quality of the 3-eq model is better than the 2-eq approach and is quite satisfactory with regards to its simplicity and low CPU cost. This model is then a good candidate to estimate soot production using LES of complex industrial applications and it can be used to perform parametric studies necessary for engineering design whose CPU cost is today prohibitive with other models.

## 4.2. NDF reconstruction

### 4.2.1. Laminar flames

The NDF reconstruction is validated *a priori* on two laminar flame simulations using the SM [12]: a premixed flame stabilized by a stagnation plate and a counterflow diffusion flame. The spatial evolutions of  $f_v$  and  $N_s$  are presented in Fig. 4. The two flame profiles greatly differ, leading to a large variability of the NDF.  $f_v$  and  $N_s$  have been extracted at six different positions along both flames, identified by the vertical lines in Fig. 4, to calculate  $v_s$ . The NDF is then re-

constructed at six locations as  $N_s \bar{n}_a(v)$  and compared to the NDF provided by the SM in Fig. 5. The reconstructed NDF (R-NDF) reproduces the expected behavior, the Pareto and the LN functions mainly contributing to small and large particles, respectively. The R-NDF also correctly guarantees the first two moments, i.e.  $N_s$  and  $f_v$ , with a maximum error of about 10%, and captures very well the transition between one-peak to two-peak shapes for the two different flame structures.

#### 4.2.2. Turbulent flames

As a final validation, the R-NDF is tested on a turbulent ethylene/air jet flame (Fig. 6, [23]). The temporal and spatial evolutions of the NDF have been characterized using SM [13]. Here, an instantaneous solution of the SM is used to

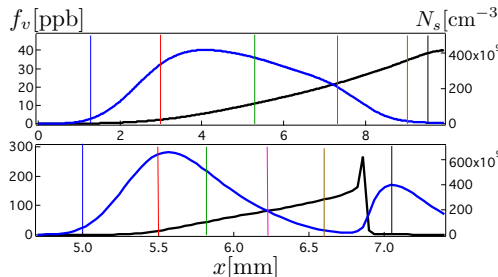


Figure 4: Spatial evolution of  $f_v$  (black) and  $N_s$  (blue) obtained with the sectional method [12] for a premixed (top) and a diffusion (bottom) flame. Vertical lines indicate the axial position of the NDF represented in Fig. 5.

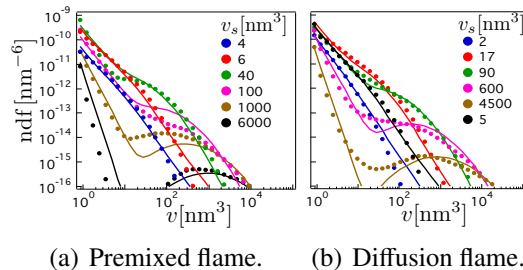


Figure 5: Validation of the NDF reconstruction model on laminar flames: the reconstructed NDF (lines) is compared to the sectional NDF (symbols) at 6 different positions indicated in Fig. 4.

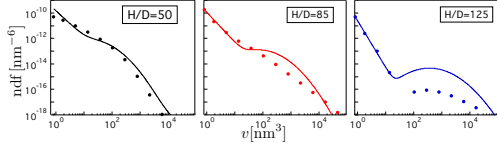


Figure 6: Validation of the NDF-reconstruction model on a turbulent jet flame: R-NDF (lines) is compared to the sectional NDF (symbols) from an instantaneous solution along the central axis [23] at 3 axial positions  $H/D = 50, 85, 125$  for which  $v_s = 40, 250$  and  $2000 \text{ nm}^3$ .

compare the R-NDF and sectional NDF on the central axis at three flame heights  $H/D = 50, 85$  and  $125$ , where  $D = 3.2 \text{ mm}$  is the fuel injector diameter of the main jet. The 3-eq model provides a good prediction of the spatial transition from one-peak to two-peaks shapes of the NDF.

To conclude, it should be reminded that the reconstruction procedure depends not only on the global transported quantities but also on some parameters ( $\alpha$ ,  $\sigma$  and  $\bar{n}_1^0$ ) fitted in Sec. 3 on a specific flame from the results obtained with a specific SM. Even if this reconstruction has been validated a priori on different flame archetypes, a different evolution of the NDF with  $v_s$  may be observed for different soot modes, fuels or operating conditions. However, the decomposition of the NDF into a Pareto and a LN distribution seems to be a general strategy to represent the NDF without the transport of additional information, allowing parametric studies on gas turbines at low CPU cost.

## 5. LES of the FIRST combustor

The 3-eq model is now used to perform an LES of soot production in the model combustor FIRST, investigated experimentally at DLR [10]. Once the simulation is validated against the experimental data, results on the PSD validity are discussed.

### 5.1. Numerical setup

The FIRST configuration of DLR [10] is a classical benchmark for validation of soot modelling [3, 7, 8, 24, 25]. The burner consists in a plenum, a swirler and a combustion chamber. Ethylene and air are injected separately and mixed directly in the chamber where a swirled flame is stabilized.

The case studied here corresponds to a pressure of 3 atm, an injection equivalence ratio of  $\phi_{\text{inj}} = 1.2$  and a secondary air injection reducing the global equivalence ratio down to  $\phi_{\text{global}} = 0.86$ . Simulation is performed with the AVBP solver [26]. The flow is simulated on the 40 million tetrahedra unstructured mesh presented in [27]. Adiabatic no-slip walls are considered except for the chamber walls, whose temperature is imposed based on experiments [28]. A look-up table based on the RFPV model [29] is built from the KM2 [21] detailed mechanism, to obtain information on gaseous species, as well as on precursors and on gaseous quantities required for the solid phase. Turbulent subgrid stresses are modeled using the WALE approach [30], with constant turbulent Prandtl and Schmidt numbers ( $Pr_t = Sc_{t,k} = 0.6$ ). The subgrid chemical source terms of gaseous species are described using a  $\beta$ -pdf model [31]. The intermittency model for subgrid soot source terms developed in [32] for HMOM is used here. An optically-thin model is used for radiation. Time-averaged quantities have been obtained over 30 ms, corresponding to approximately six convective times. The gas phase simulation has already been validated in [33], showing a negligible impact of soot radiation on the gas phase. Therefore, the validation of the gas phase is not presented here and only results on soot are discussed.

## 5.2. Analysis of results

Results on time-averaged  $f_v$  using the 3-eq and SM [33] models are shown in Figs. 7(a)-7(b) and compared to the experimental data (Fig. 7(c)). To ease the comparison, the experimental and numerical results have been normalized by their respective maximum values ( $f_v^{\max,\text{exp}} = 30 \pm 9$  ppb,  $f_v^{\max,\text{num}} = 10$  ppb). The quality of the prediction of the 3-eq model (Fig. 7(a)) is very satisfactory compared to the SM (Fig. 7(b)), for a CPU cost reduced by a factor 3. It should be noticed that in the SM an empirical relation was imposed to account for fractility [13], whereas the total particle surface is transported in the 3-eq model. Thus, the surface reactions may differ between the two calculations, modifying the production of  $f_v$ , so that any deeper comparison between the two models would not be pertinent.

Soot localization is correctly detected, but there is a factor 3 between experiments and simulations. Experimentally, the soot yield assumes the same level all along the flame and decreases for  $y > 60$  mm. On the contrary, the numerical results predict a high value only for  $y < 40$  mm and rapidly decreases downstream. The quality of these results is overall satisfactory since the prediction of  $f_v$  is extremely challenging and the experimental data is characterized by an error of 30%.

The temporal evolution of global values of  $N_s$ ,  $f_v$  and  $v_s$  are represented in Fig. 8(a) at the point of maximum  $f_v$  fluctuations ( $x = 12$  mm,  $y = 24$  mm) showing that  $v_s$  highly fluctuates with time. In Fig. 8(b), the PSD obtained through the reconstruction procedure is represented for the three times indicated in Fig. 8(a). As expected, it can be observed that the PSD shape greatly varies in time. However, the time-averaged distribution has almost everywhere a one-peak shape (not shown), as observed in the SM simulation [33]. This differentiates soot produc-

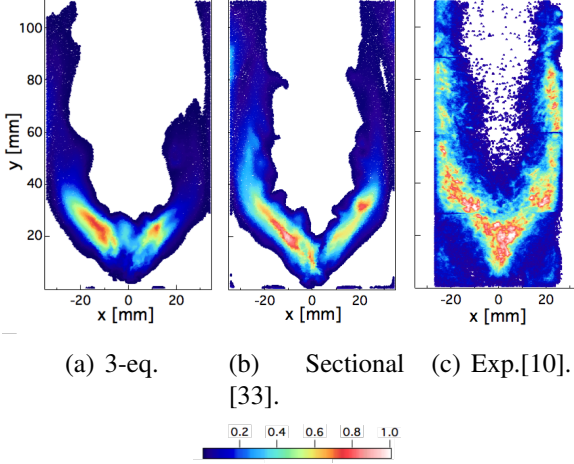
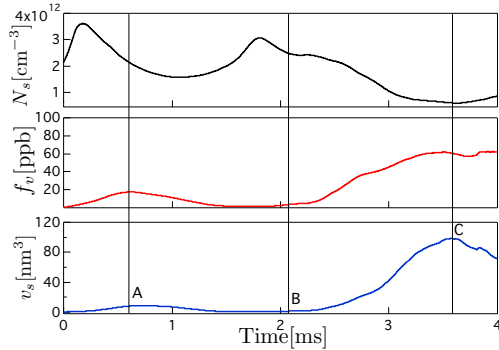
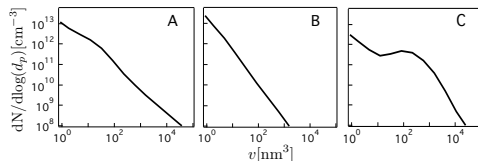


Figure 7: Time-averaged  $f_v$  normalized by its maximum value:  $\bar{f}_v = f_v/f_v^{\max}$ . Results from the 3-eq (a) and the sectional (b, [33]) methods ( $f_v^{\max,\text{num}} = 10 \text{ ppb}$ ) are compared to experiments (c,  $f_v^{\max,\text{exp}} = 30 \pm 9 \text{ ppb}$ , [10]).



(a) Time evolution of global quantities.



(b) Reconstructed local PSD.

Figure 8: Temporal evolution of (a)  $N_s$ ,  $f_v$ ,  $v_s$  and (b) PSD at three instants for the 3-eq model at  $x = 12 \text{ mm}$  and  $y = 24 \text{ mm}$ .

tion in this configuration from what has been observed in the turbulent jet flames [13, 18, 19] and can be explained by the strong correlation evidenced between small (high) soot levels and one- (two)-peak distributions [13]. By looking at experimental results, a one-peak PSD is expected in this configuration since soot yield is of the order of a particle per billion, compared to ppm observed in jet flames.

Concerning alternative reconstruction techniques to obtain time-averaged PSD, Rittler et al. [34] suggested to use temporal fluctuations of  $v_s$  from a mono-disperse model. This strategy was applied to the investigation of the titanium oxide population in a turbulent flame. However, there is no proof that the temporal evolution of  $v_s$  is representative of the time-averaged PSD. To evidence it, the time-averaged PSD for the data presented in Fig. 8 is shown in Fig. 9 (solid line), along with the temporal fluctuations of  $v_s$  (histogram). It shows that the number of particles is underestimated for the biggest particles because the mean volume  $v_s$  will obviously never be able to reach the volumes encountered in the tail of the PSD. Therefore, tracing the temporal evolution of  $v_s$  (or other moments) is not a pertinent representation of time-averaged PSD: a R-NDF or transported NDF are necessary. Another strategy may be to recalculate the PSD from the time-averaged  $v_s$  instead of simply reporting  $v_s$  fluctuations. This is represented in Fig. 9 (dashed line), showing that it is not identical to the time-averaged PSD. This is again not surprising because of the high non-linearity of the reconstruction with respect to moments. It can therefore be conclude that the only way to get the time-averaged PSD is to store the temporal evolution of the PSD (reconstructed or transported).

In conclusion, the 3-eq model provides good prediction of soot global quantities with no fitting procedure for parameters governing soot production processes.

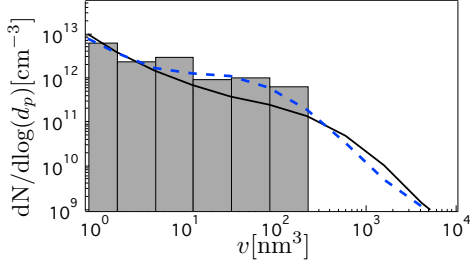


Figure 9: Time-averaged R-PSD with the 3-eq model (continuous black line) is compared to temporal fluctuations of the mean particle volume (histogram, [34]) for the data presented in Fig. 8. The PSD reconstructed from the time-averaged mean particle volume is also represented in dashed blue line.

Concerning the PSD reconstruction, it should be noticed here that no validation has been provided on turbulent flames by comparison with experimental data, since they are today not available for this configuration. However, it represents a low-cost procedure to get information on the NDF, which cannot be represented only by looking to the fluctuations of  $v_s$ .

## 6. Conclusion

A simple 3-eq model for the description of soot production has been proposed based on a mono-disperse closure of the source terms of a sectional method. It presents the following advantages: the addition of a transport equation for the total soot surface guarantees a better description of surface reactions compared to the semi-empirical method; its theoretical development guarantees a larger validity of the model; it can easily be implemented into CFD solvers and provides a reasonable estimation of the PSD for a low CPU cost (the cost of a LES of a turbulent sooting flame is approximately reduced by a factor 3 compared to the sectional method using 25 sections when using a tabulation technique for gas description).

However, the NDF reconstruction still requires more validation and the accu-

racy of the 3-eq model is expected to be reduced when the NDF is highly polydisperse. Nevertheless, since a correlation seems to exist between small values of  $f_v$  (less than ppm) and one-peak NDF, the mono-disperse model proposed here is a good candidate for LES of sooting turbulent flames of gas turbines and aeronautical burners, where the produced instantaneous  $f_v$  is expected to be small (i.e. less than ppm).

## Acknowledgments

This work was granted access to the HPC resources of CINES under the allocation x20162b6172 of GENCI (Grand Equipement National de Calcul Intensif). CERFACS is also gratefully acknowledged for providing the AVBP code and the mesh of the FIRST configuration.

## References

- [1] K. Leung, R. Lindstedt, W. Jones, Combust. Flame 87 (1991) 289 – 305.
- [2] G. Lecocq, D. Poitou, I. Hernandez, F. Duchaine, E. Riber, B. Cuenot, Flow, Turb. and Combustion 92 (2014) 947–970.
- [3] B. Franzelli, E. Riber, B. Cuenot, M. Ihme, Proceedings of ASME Turbo Expo GT2015-43630, Montreal, Canada (2015).
- [4] M. Mueller, G. Blanquart, H. Pitsch, Combust. Flame 156 (2009) 1143 – 1155.
- [5] M. Frenklach, Chem. Engr. Sci. 57 (2002) 2229–2239.
- [6] M. Mueller, H. Pitsch, Physics of Fluids 25 (2013) 110812.

- [7] H. Koo, V. Raman, M. Mueller, K. Geigle, 53rd AIAA Aerospace Sciences Meeting (2015).
- [8] A. Wick, F. Priesack, H. Pitsch, Proceedings of ASME Turbo Expo GT2017-63293, Charlotte, USA (2017).
- [9] M. Grader, C. Eberle, P. Gerlinger, M. Aigner, Proceedings of ASME Turbo Expo GT2018-75254, Oslo, Norway (2018).
- [10] K.-P. Geigle, R. Hadef, W. Meier, Proceedings of ASME Turbo Expo paper GT2013-95316, San Antonio, Texas (2013).
- [11] B. V. Derjaguin, A. I. Storozhilova, Y. I. Rabinovich, *J. Colloid Interf. Sci.* 21 (1966) 33–58.
- [12] P. Rodrigues, B. Franzelli, R. Vicquelin, O. Gicquel, N. Darabiha, *Proc. Combust. Inst.* 36 (2017) 927–934.
- [13] P. Rodrigues, B. Franzelli, R. Vicquelin, O. Gicquel, N. Darabiha, *Combust. Flame* 190 (2018) 477–499.
- [14] S. Friedlander, C. Wang, *J. Colloid Interf. Sci.* 22 (1966) 126–132.
- [15] A. Kelesidis, E. Goudeli, S. E. Pratsinis, *Proc. Combust. Inst.* 36 (2017) 29–50.
- [16] F. Jun, S. Xueming, Y. Hongyong, Z. Xin, *Fire Sci.* 22 (2004) 53–68.
- [17] A. D. Abid, N. Heinz, E. D. Tolmachoff, D. J. Phares, C. S. Campbell, H. Wang, *Combust. Flame* 154 (2008) 775 – 788.

- [18] W. Boyette, S. Chowdhury, W. Roberts, Flow, Turb. and Combustion 98 (2017) 1173–1186.
- [19] S. Chowdhury, W. Boyette, W. Roberts, J. Aerosol Sci. 106 (2017) 56–67.
- [20] B. Franzelli, B. Fiorina, N. Darabiha, Proc. Combust. Inst. 34 (2013) 1659–1666.
- [21] Y. Wang, A. Raj, S. Chung, Combust. Flame 160 (2013) 1667–1676.
- [22] Sweep2: Cambridge soot simulator, cambridge, <http://como.cheng.cam.ac.uk>, 2006.
- [23] C. Shaddix, J. Zhang, R. Schefer, J. Doom, J. Oefelein, S. Kook, L. Pickett, H. Wang, Understanding and Predicting Soot Generation in Turbulent Non-Premixed Jet Flames, Technical Report, Sandia Report SAND2010-7178, 2010.
- [24] C. Eberle, P. Gerlinger, K. Geigle, M. Aigner, Combust. Sci. Tech. 187 (2015) 1841–1866.
- [25] F. Dupoirieux, N. Bertier, Int. J. Sust. Aviation 2 (2016).
- [26] N. Gourdain, L. Gicquel, M. Montagnac, O. Vermorel, M. Gazaix, G. Staffelbach, M. García, J.-F. Boussuge, T. Poinsot, Comput Sci Discov. 2 (2009) 015003.
- [27] A. Felden, E. Riber, B. Cuenot, Combust. Flame 191 (2018) 270 – 286.
- [28] P. Nau, Z. Yin, K. P. Geigle, W. Meier, Appl. Phy. B 123 (2017) 1–8.
- [29] M. Ihme, H. Pitsch, Physics of Fluids 20 (2008) 055110.

- [30] F. Nicoud, F. Ducros, Flow, Turb. and Combustion 62 (1999) 183–200.
- [31] F. Lien, H. Liu, E. Chui, C. McCartney, Flow, Turb. and Combustion 83 (2009) 205–226.
- [32] M. Mueller, H. Pitsch, Phys. Fluids 23 (2011) 409 – 418.
- [33] P. Rodrigues, Multi-physics modelling of turbulent sooting flames including thermal radiation and wall heat transfer, Ph.D. thesis, Université Paris-Saclay, 2018.
- [34] A. Rittler, L. Deng, I. Wlokas, A. Kempf, Proc. Combust. Inst. 36 (2017) 1077–1087.